PHYSICAL REVIEW B VOLUME 40, NUMBER 10 1 OCTOBER 1989

Analysis of Bloch-wall fine structures by magnetic force microscopy

U. Hartmann
Institut für Schicht- und Ionentechnik der Kernforschungsanlage Jülich GMBH, D-5170 Jülich, Federal Repubic of Germany
(Received 22 May 1989)

Microfield profiles of isolated 180° Bloch walls in highly perfect iron single crystals have been detected using a magnetic force microscope (MFM). The achieved spatial resolution of 10 nm permits a first quantitative insight into the near-surface variation of the stray field. A closer analysis of the experimental data by comparison with model calculations confirms some fundamental uncertainties in image interpretation generally inherent to the MFM technique. The basic problems are summarized as a general guideline for the applicability of the MFM technique.

Further success in magnetic material improvement and device miniaturization is based strongly on the availability of high-resolution magnetic imaging techniques. Recently, a detection method with submicrometer resolution has been proposed[1,2] which is based on a modified version of the scanning tunneling microscope.[3] In a magnetic force microscopy (MFM), interactions between a sharp magnetic tip and the microfield distribution of a ferromagnetic sample are detected. So far, the domain structure from different samples of current interest in magnetic technology has been studied achieving resolutions between 100 and 10 nm.[1,2,4,5]

However, in all these experiments MFM image interpretation turns out to be more speculative than rigorously quantitative. The problem results from two basic difficulties. First, the micromagnetic spin configuration under investigation, e.g., of Bloch walls, is *a priori* not known in detail. The problems in rigorously solving the micromagnetic equations under realistic boundary conditions are well known.[6] The second difficulty is the unknown domain configuration of the ferromagnetic microscope tip which determines the actual response of the probe. Thus, MFM images are generally complex convolutions of the sample and probe magnetic properties and the image interpretation is not straightforward.[7]

This paper is focused on an elucidation of the basic problems underlying image interpretation in MFM. For this purpose we have chosen an isolated well-defined micromagnetic object: The 180° Bloch-type boundary in a highly perfect iron whisker single crystal. This configuration has been investigated for a long time and in great detail by extensive theoretical analysis[8-11] as well as by various experimental methods.[12-15] However, up to the present, neither a theoretical solution nor a detailed experimental result has been presented concerning the exact stray-field variation in the near-surface range of such walls.

The experimental investigations have been performed with a compact MFM which was operated in ambient air at room temperature. Local imaging of probe-sample interactions is based on detection of the actual compliance $D = \partial F/\partial z$, where F is the vertical force component acting between probe and sample. D can be detected in the following way: The sample is attached to a bimorph piezoplate. The microscope probe is positioned a few nanometers above the sample surface and periodically deflected by a few Angstroms in the z direction, i.e., vertically with respect to the sample surface. Modulation of the probe-sample distance causes, via interaction forces, microscopic deflections of the sample-holder piezo. Lock-in detection of the induced voltage then yields a direct measure of the probe-sample compliance D. Using an appropriate feedback-loop system, images of constant D are obtained. Details of the employed experimental setup have been published elsewhere.[16]

Measurements on various nonmagnetic probe-sample systems have confirmed that even in the absence of long-range magnetostatic interactions a compliance is detectable up to probe-sample distances of some tens of nanometers.[17] The origin of this long-range tip-sample coupling is not yet understood. However, use of this ever present compliance contribution as a control parameter for the MFM feedback loop permits a reproducible adjustment of the probe at the desired probe-sample distance.

To obtain a magnetic contrast, ferromagnetic tips have been fabricated from iron wires by electrochemical etching.[16] The single-crystal iron whiskers used as samples were prepared by hydrogen reduction of ferrous chloride.[15] They exhibit a ⟨100⟩ growing direction and are bounded by {100} crystallographic faces. The Landau domain configuration is usually composed of a long 180° Bloch wall along ⟨100⟩ and of 90° flux-closure domains at the crystal tips.[15] An exact positioning of the microscope probe with respect to the 180° Bloch wall could be achieved by magneto-optic Kerr observations during MFM operation.[16]

In a first experiment, successive equicompliance scans have been performed across a 180° Bloch wall. As shown in Fig. 1, the wall running along ⟨100⟩ yields a clear contrast. The induced deflection of the probe is roughly 1 nm, while the overall compliance noise amounts to about 0.2 nm.

In a further experiment with higher lateral resolution, 20 line scans across the wall have been averaged to obtain a more detailed profile of the wall microfield some ten nanometers above the whisker surface. As shown in Fig. 2, the total profile is clearly asymmetric. The lateral microfield extent amounts to more than 500 nm corresponding to about twice the bulk wall width in iron whiskers.[14]

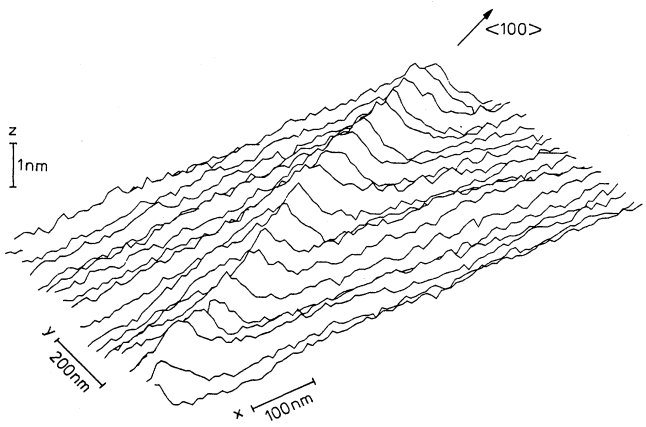

FIG. 1. Equicompliance MFM contrast of a 180° Bloch wall in an iron whisker running in ⟨100⟩ crystallographic direction.

The basic question with respect to a micromagnetic interpretation of the above data is the following: In which way is the recorded image of the wall profile influenced by probe properties? In order to elucidate this problem on a quantitative level, the magnetostatic probe-sample interactions have to be calculated introducing the probe and sample magnetization configurations. Because of the complex structure of the underlying micromagnetic equations[6] and the somewhat uncertain boundary conditions concerning the exact probe geometry, a rigorous solution of the micromagnetic problem seems impossible.[7,18] Thus, we have to employ sufficiently simple models allowing for a characterization of the basic MFM contrast mechanism.

Completely ignoring the actual spin configuration, the intersection of the 180° Bloch wall with the sample surface is simply represented by an inhomogeneously charged stripe as shown in the inset of Fig. 3. This model has already proven useful for an interpretation of Bitter pattern evaluation.[19] The microfield components resulting from this simplified model are given by[11]

$$H_x(x,z) = \frac{M}{2\pi}\int_{-\pi/2}^{\pi/2} d\theta \tan\theta\, w_\theta(x,z)\,, \tag{1a}$$

$$H_z(x,z) = \frac{M}{2\pi}\int_{-\pi/2}^{\pi/2} d\theta\, w_\theta(x,z)\,, \tag{1b}$$

where M is the saturation magnetization and

$$w_\theta(x,z) = 1/\cosh[q/\delta(x+z\tan\theta)]\,. \tag{1c}$$

Material parameters entering Eq. (1c) are the quality factor $q=(M/2H_K)^{1/2}$ given by the saturation magnetization M and the anisotropy field H_K, and the exchange length $\delta=(A/K)^{1/2}$ determined by the exchange constant A and the anisotropy constant K.

The two-dimensional field variations evaluated numerically according to Eqs. (1) are plotted in Fig. 3. While the horizontal field component H_x vanishes directly on the sample surface $z=0$, the vertical component $H_z(x)$ corresponds to the distribution of magnetic charges produced by the hypothetical wall configuration.

The next step in our model calculations is an adequate characterization of the MFM probe on the applied mesoscopic magnetostatic level. Electrochemically prepared

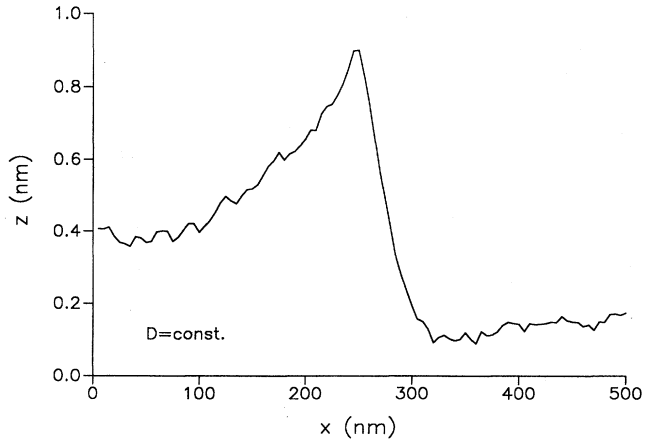

FIG. 2. High-resolution image of the wall profile obtained in the equicompliance mode.

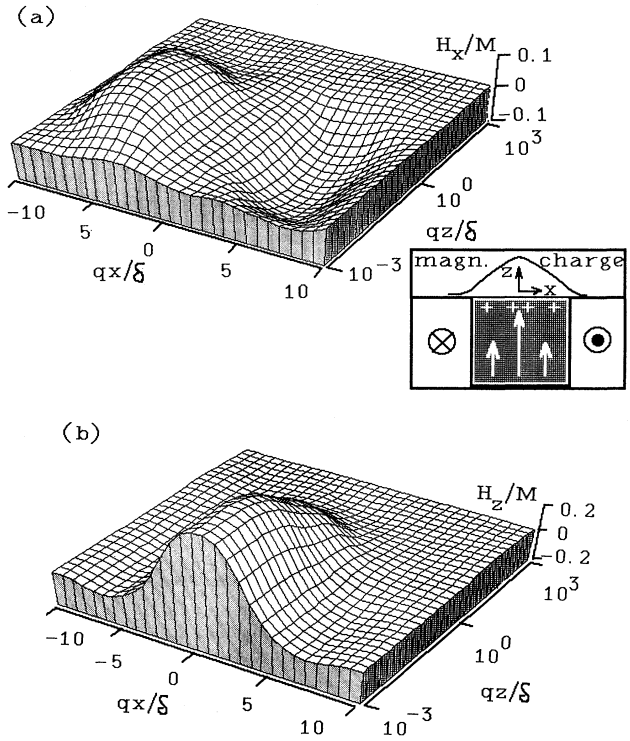

FIG. 3. Microfield profile of the hypothetical wall model employed for the calculations. (a) The inset shows the basic geometry and schematically illustrates the charge distribution at the intersection of the wall with the sample surface. The horizontal field component H_x is plotted with respect to reduced coordinates. Note the logarithmic scale in the z direction. (b) Corresponding vertical field component H_z.

probes generally exhibit a somewhat irregular geometry as shown in Fig. 4(a). Because of natural shape anisotropy, the preferred magnetization direction at the apex is parallel to the tip axis, while bulk domains largely exhibit an internal flux closure forced by overall stray-field minimization. The net magnetic response of the MFM probe is thus determined by the volume and actual orientation of the apex domain.[7] Because of imperfect probe preparation or attachment, the magnetic moment is generally not exactly parallel to the z direction; i.e., it exhibits additional x,y components with respect to the sample coordinates [see Fig. 4(a)]. In order to characterize the above properties, we approximate the magnetic detector by a cuboidal, homogeneously magnetized domain with the free parameters given by the dimensions l_x,l_y,l_z and by the orientation of the net magnetic moment $\mathbf{m}$, i.e., by m_x,m_y,m_z, with $m_x^2+m_y^2+m_z^2=1$, as shown in Fig. 4(b). Representation of the mesoscopic probe properties by this simple model makes further calculations straightforward.[20]

Subjected to a microfield $\mathbf{H}(\mathbf{r})$, the magnetostatic potential of the probe is given by

$$\Phi(\mathbf{r}) = -\mu_0 \int\int\int_{\text{probe}} \mathbf{m}\cdot\mathbf{H}(\mathbf{r}'+\mathbf{r})d^3r', \tag{2}$$

where integration is extended over the cuboidal domain shown in Fig. 4(b). The experimentally detectable compliance is then given by

$$D(\mathbf{r}) = \partial^2\Phi(\mathbf{r})/\partial z^2. \tag{3a}$$

Combination of Eqs. (1), (2), and (3a) yields

$$D(\mathbf{x},\mathbf{z}) = D_0 \int_{-\pi/2}^{\pi/2} d\theta \tan\theta[\alpha+(1-\alpha^2)^{1/2}\tan\theta] \times \{[w_\theta(\mathbf{x},\mathbf{z})]_{x-l_x/2}^{x+l_x/2}\}_z^{z+l_z}, \tag{3b}$$

with $D_0=(\mu_0/2\pi)mMl_y$ and the actual probe magnetization $m_x/m=(1-\alpha^2)^{1/2}$, $m_y=0$, and $m_z/m=\alpha$.

At given values of $q=4.3$ and $\delta=20$ nm for the quality factor and the exchange length of iron, the above relation for the compliance D contains the probe properties α,l_x,l_z and the probe-sample distance z as free parameters to be fitted against the experimental data from Fig. 2. The result obtained for $\alpha=0.6$, $l_x=5$ nm, $l_z=456$ nm, and $z=93$ nm is shown in Fig. 5.

The asymmetry of the obtained profile is caused by an inclination of $\arctan[(1-\alpha^2)^{1/2}/\alpha]=52.5°$ of the probe magnetic moment $\mathbf{m}$ with respect to the z coordinate of the sample as shown in Fig. 4(b). Thus, both field components H_x and H_z shown in Fig. 3 contribute to the MFM contrast. The geometric dimensions $l_x=5$ nm and $l_z=465$ nm indicate an elongated domain located at the probe apex which seems reasonable due to shape anisotropy.[7] As a consequence of the electrochemical preparation procedure we may further assume a symmetrical cross section of the probe; i.e., $l_y=l_x$. Thus, we find $D_0=3mN/m$ for the compliance constant in Eq. (3b). The absolute compliance variations derived from Fig. 5 are then in the range of $\mu N/m$ at a working distance of $z=93$ nm.

However, in spite of the surprisingly good agreement between experiment and theory we have to ask for the relevance of our model calculations. It should be recalled that these calculations are based, on the one hand, on a wall model which is definitely inadequate with respect to the actual micromagnetic situation[8] and, on the other

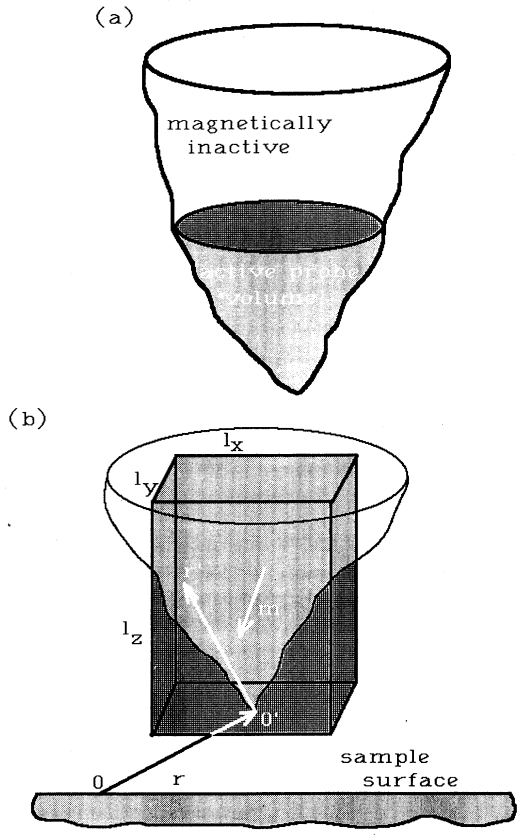

FIG. 4. (a) Schematic sketch of an electrochemically prepared MFM probe. (b) Simplified model of the probe used for the calculations.

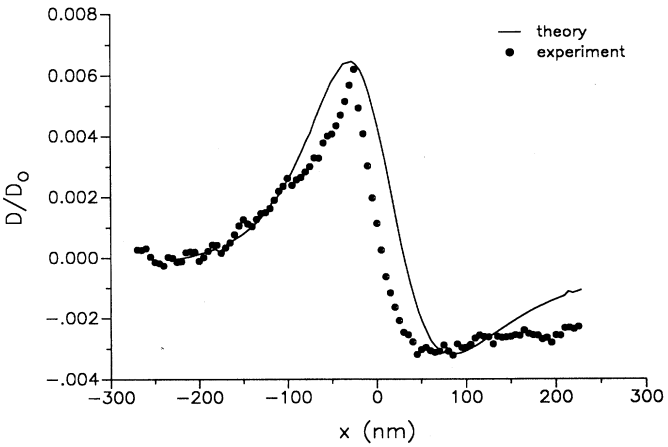

FIG. 5. Comparison between experimentally and theoretically obtained results for the wall profile.

hand, on a rigorously simplified probe model. The reason for this discrepancy is obvious: The employed model configuration roughly characterizes the experimental situation on a mesoscopic level corresponding to a first-order approximation. However, the model apparently contains sufficient variational parameters to account for second-order effects, i.e., fine-structure details of the wall and the microscope probe itself.

Since this latter aspect of the MFM image interpretation is not sufficiently considered in most of the work on this matter, we should conclude with some constraining guidelines of general validity to MFM analysis of micromagnetic objects:

(i) To a first-order approximation of experimental MFM data the *a priori* unknown mesoscopic properties of the probe can be characterized by a geometrically simple model, e.g., such as in Fig. 4(b). Such a model contains sufficient free parameters to roughly characterize an MFM image on a purely magnetostatic level, but does not permit image interpretation on a micromagnetic level. Simple point-dipole approximation of the probe[21] is generally inadequate because it does not really account for long-range magnetostatic interactions.

(ii) If neither the probe nor the microfield configuration is known in detail, none of them can be determined by MFM. An experimentally obtained image can be simulated by an infinite number of microfield configurations if the probe parameters are suitably chosen: The asymmetric profile in Fig. 5 can be either produced by an asymmetric spin configuration of the wall[8] or by a tilted probe position as discussed above.

(iii) If the probe magnetic configuration is known in detail, the microfield profile can, in principle, be determined. However, a deconvolution of the field components H_x, H_y,H_z is not possible since there is no unequivocal relation between the MFM signal and the successive components [see Eq. (3b)].

(iv) If the microfield profile of a magnetic structure is known, MFM imaging at a known working distance permits a calibration of the probe. Mesoscopic geometric and magnetic information are obtained in terms of the probe model, e.g., that in Fig. 4(b), initially employed.

Under consideration of the above guidelines, the present experiment should be considered as a first high-resolution but semiquantitative analysis of the near-surface microfield resulting from an isolated Bloch wall. A rigorously quantitative measurement would require more detailed information on the employed MFM probe. In the future, well-defined MFM probes might be obtainable if improved and reproducible fabrication techniques such as nanometer lithography are employed.

Thanks are due to T. Göddenhenrich for performing the MFM experiments and to M. Anders for his technical assistance. Valuable discussions with C. Heiden are gratefully acknowledged.

[1]J. J. Sáenz, N. García, P. Grütter, E. Meyer, H. Heinzelmann, R. Wiesendanger, L. Rosenthaler, H. R. Hidber, and H. J. Güntherodt, J. Appl. Phys. **62**, 4293 (1987).

[2]Y. Martin and H. K. Wickramasinghe, Appl. Phys. Lett. **50**, 1455 (1987).

[3]G. Binnig, C. F. Quate, and Ch. Gerber, Phys. Rev. Lett. **56**, 930 (1986).

[4]P. Grütter, E. Meyer, H. Heinzelmann, L. Rosenthaler, H. R. Hidber, and H. J. Gütherodt, J. Appl. Phys. **63**, 2947 (1988).

[5]Y. Martin, D. Rugar, and H. K. Wickramasinghe, Appl. Phys. Lett. **52**, 244 (1988).

[6]W. F. Brown, *Micromagnetics* (Wiley, New York, 1963).

[7]U. Hartmann, J. Appl. Phys. **64**, 1561 (1988).

[8]A. Hubert, *Theorie der Domänenwände in Geordneten Medien* (Springer-Verlag, Berlin, 1974).

[9]U. Hartmann, Phys. Status Solidi (a) **101**, 22 (1987).

[10]U. Hartmann, J. Appl. Phys. **62**, 621 (1987).

[11]U. Hartmann, Phys. Status Solidi (b) **151**, 289 (1989).

[12]T. Suzuki and H. Suzuki, IEEE Trans. Magn. **MAG-13**, 1505 (1977).

[13]U. Hartmann and H. H. Mende, J. Phys. D **18**, 2285 (1985).

[14]U. Hartmann and H. H. Mende, Phys. Rev. B **33**, 4777 (1986).

[15]U. Hartmann and H. H. Mende, J. Appl. Phys. **59**, 4123 (1986).

[16]T. Göddenhenrich, U. Hartmann, M. Anders, and C. Heiden, J. Microsc. **152**, 527 (1988).

[17]M. Anders and C. Heiden, J. Microsc. **152**, 643 (1988).

[18]U. Hartmann and C. Heiden, J. Microsc. **152**, 281 (1988).

[19]U. Hartmann, J. Magn. Magn. Mater. **68**, 298 (1987).

[20]U. Hartmann, Phys. Status Solidi (a) **115**, 822 (1989).

[21]U. Hartmann, Phys. Lett. A **137**, 475 (1989).